

# Experimental evidence of antiproton reflection by a solid surface

A. Bianconi,<sup>1,2</sup> M. Corradini,<sup>1,2</sup> A. Cristiano,<sup>1</sup> M. Leali,<sup>1,2</sup>  
E. Lodi Rizzini,<sup>1,2</sup> L. Venturelli,<sup>1,2</sup> N. Zurlo,<sup>1,2</sup> and R. Donà<sup>3</sup>

<sup>1</sup>*Dipartimento di Chimica e Fisica per l'Ingegneria e per i Materiali, Università di Brescia, 25133 Brescia, Italy*

<sup>2</sup>*Istituto Nazionale di Fisica Nucleare, Gruppo Collegato di Brescia, 25133 Brescia, Italy*

<sup>3</sup>*Dipartimento di Fisica dell'Università di Bologna and INFN Sezione di Bologna, 40127 Bologna, Italy*

(Dated: October 30, 2018)

We report here an experimental evidence of the reflection of a large fraction of a beam of low energy antiprotons by an aluminum wall. This derives from the analysis of a set of annihilations of antiprotons that come to rest in rarefied helium gas after hitting the end wall of the apparatus. A Monte Carlo simulation of the antiproton path in aluminum indicates that the observed reflection occurs primarily via a multiple Rutherford-style scattering on Al nuclei, at least in the energy range 1-10 keV where the phenomenon is most visible in the analyzed data. These results contradict the common belief according to which the interactions between matter and antimatter are dominated by the reciprocally destructive phenomenon of annihilation.

PACS numbers: 36.10.-k, 68.49.Sf, 13.40.-f

## I. INTRODUCTION

A large part of the experimentation with antiprotons after the 80's has been devoted to the low energy interactions and properties of the antimatter-matter systems [1]. Among the other ones, this has produced relevant results concerning the  $\bar{H}$  production [2, 3] and the properties of antimatter-matter systems on an atomic or molecular scale [4, 5, 6]. In this paper we present the experimental evidence of the reflection of a conspicuous fraction (20-30%) of a beam of low energy (magnitude 1-10 keV) antiprotons hitting a solid surface. This contradicts the common belief according to which the interactions between antiprotons and matter at low energies are dominated by annihilations. The present analysis can be considered a refinement of the data analysis we presented in [7]. Although the data were presented there, only a part of them was explained in that work.

The experimental evidence refers to antiprotons that are reflected with energy  $\sim$  a few keV, by a wall of solid aluminum. At these energies, the simulation of the reflection process shows that it is dominated by multiple Rutherford-like “large angle” scattering, where “large” means some tenths degrees. According to our simulation, the reflected fraction should increase at decreasing energy, possibly reaching 50% at 500 eV.

One century ago E. Rutherford wrote [8] about the “diffuse reflection” of  $\alpha$  and  $\beta$  particles by thin metal layers, observing that the electromagnetic aspects of the process did not depend on the charge sign of the colliding particles. In the  $\bar{p}$ -nucleus case however the Rutherford mechanism competes with the annihilation process. At a different mass scale, it has been shown that positrons implanted into a variety of metals may return to the surface where they are re-emitted into the vacuum, possibly after capturing electrons and forming complex structures (see [9, 10] and references therein). Such processes may occur if the diffusion length is longer than the implantation depth. A similar situation takes place in the case

considered here, where at the relevant energies 1-10 keV both the stopping range and the annihilation free path of the  $\bar{p}$  in aluminum are longer than the path needed to lose memory of the initial flight direction.

## II. THIS MEASUREMENT

The data considered here belong to a set of measurements performed at the LEAR (Low Energy Antiproton Ring) decelerator at CERN within the PS201 (OBELIX) experiment [11]. In these measurements, an antiproton beam with continuous energy distribution in the range 0-3 MeV enters a 75 cm-long aluminum vessel containing the gas target (Fig.1, see ref.[12] for details on the apparatus). As any charged particle, an antiproton that is travelling in matter loses progressively energy because of the stopping power of the crossed medium. It may rarely annihilate in flight, but in most cases the annihilation will take place when it is almost at rest, after the antiproton has been captured by an atom (see ref.[12] for the separation of in-flight and at-rest annihilations). Antiprotons with entrance energy  $\lesssim$  4 keV come to rest and annihilate in the gas before reaching the end wall. Annihilation products (mesons) reach instantaneously the detectors out of the apparatus, and track interpolation allows for a precise reconstruction of the annihilation position (within cm) and time (within ns). So, the  $\bar{p}$  annihilations can be used to extract the main properties of the interactions between antiprotons and low pressure gases. In such way it has been possible to determine e.g. the  $\bar{p}$  stopping power in  $H_2$ ,  $D_2$  and He gases down to capture [7, 13, 14, 15, 16].

The data sample of the antiproton annihilations in helium at 1 mbar presented a puzzling feature left unexplained [7] up to now. This feature is visible in the “projected-path vs time” scatter plot reported in Fig.2, bottom left. Here, each point reproduces the longitudinal coordinate  $z$  and the time of an annihilation event. Fig.2,

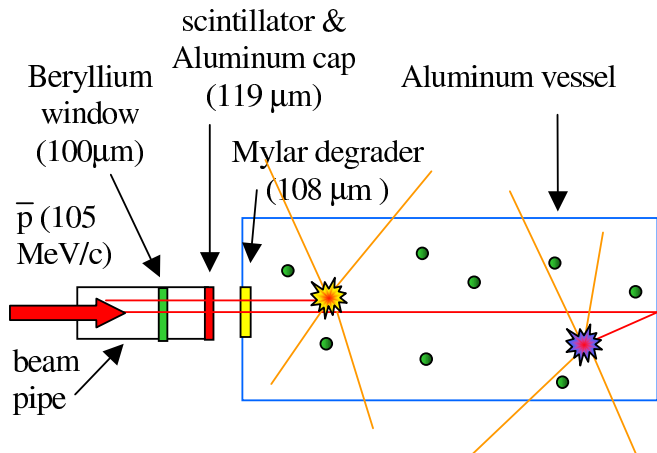


Figure 1: (Color) Layout of the beam line with antiprotons annihilation events in the target vessel.

top, pictures the composition of the scatter plot population. The structure containing most of the annihilations in the gas is the so-called Main Belt, due to antiprotons entering the vessel with energy below 3.5-4 keV, and coming to rest in gas before reaching the end wall. Initially, these particles slow down regularly because of the electronic stopping power [14]. At smaller than 0.5 keV energies, trajectory shape and energy loss are dominated by short-distance Rutherford collisions with helium nuclei and become irregular (nuclear stopping power). According to the Rutherford law the collision probability is proportional to  $\frac{1}{E^2 \sin^4(\frac{\theta}{2})}$  where  $E$  is the kinetic energy of the antiproton and the scattering angle  $\theta$  in the center-of-mass system, so large angle collisions are more likely at lower energies. Eventually, at energy below 30 eV, antiprotons are captured by helium atoms and form exotic atoms [4] with large quantum numbers. These systems undergo a statistical cascade processes leading to low-energy atomic levels within a time that depends on the density of the surrounding medium and is of the order of hundreds nanoseconds in helium at 1 mbar.

In our previous analysis [7] the Monte Carlo simulation accounted for the just described processes (i.e. interactions with gas only), and reproduced the lower edge of the Main Belt. It was however unable to reproduce the 20-30% fraction of annihilation points forming the “Backward Belt”, i.e. the large secondary structure depicted in Fig.2 (top) and evident in the data of Fig.2 bottom left.

### III. SIMULATED RECONSTRUCTION OF THE DATA SET

Recently, the Monte Carlo simulation code has been improved, including the path of the antiprotons inside the aluminum end wall. To reproduce the behavior of the antiprotons in aluminum we have used standard atomic

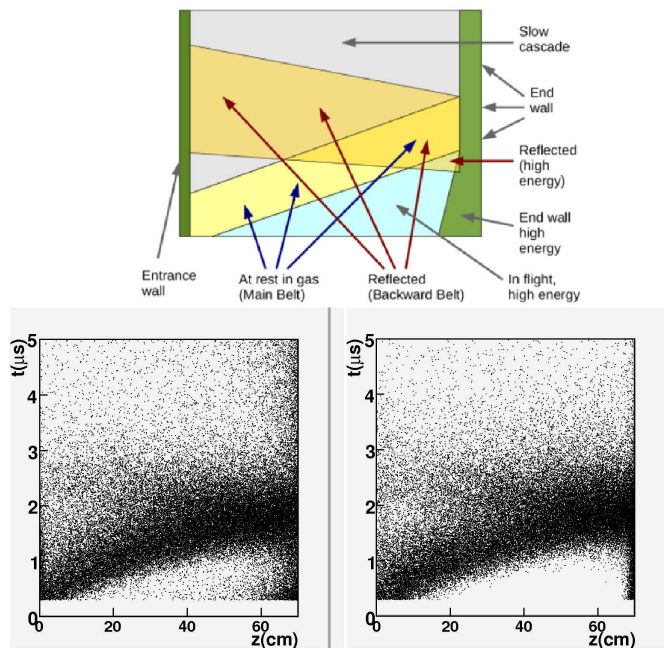


Figure 2: (Color) Top: scheme of the annihilation points of the data scatter plot (see text for explanation). Bottom left: experimental  $(z, t)$ -scatter plot. Bottom right: the simulated  $(z, t)$ -scatter plot.

and metal parameters, plus an electronic stopping power that is about a half of the corresponding function for protons in aluminum, and is very close to the one measured by ref.[17] (we have fine-tuned it on our data; for a general discussion of the behavior of charged ions in matter at low energies see ref.[18]). Below 1 keV there are no measurements of the antiproton behavior in aluminum, and we may only extrapolate the higher energy behavior (from a theoretical point of view interactions in the lower side of this region, where  $E \lesssim 100$  eV, are extremely complex, since atomic and molecular degrees of freedom play an essential role. See [19] and [20] for discussions of these points). It must be remarked that the energy region below 1 keV (in aluminum) plays a marginal role here, since antiprotons that emerge from the end wall need to cover about 20-25 cm (back in the gas) to reach a position where their annihilation may be considered a signal of their reflection.

For the electronic stopping power we use  $\frac{dE}{dx} = \alpha \times \sqrt{E}$  with  $\alpha$  normalized by  $\frac{dE}{dx} = \frac{360 \text{ MeV}}{\text{g/cm}^2}$  at  $E = 1$  keV. At a qualitative level these values are not critical, but they correspond to the best data reproduction we have tested. The scattering between antiprotons and (helium or aluminum) atoms is treated by means of a screened Rutherford potential. The screening radius of the atomic cloud is  $r_s = 1.25 \text{ \AA}$ . Moderate changes of  $r_s$  have negligible effect on the results, since the relevant collisions take place at impact parameters  $\ll r_s$ .

In the vessel, the simulated antiprotons collide on helium atoms with a probability given by the total cross

section  $\pi r_s^2$ . The electronic stopping power affects in a regular way the trajectory between two collisions, and is reproduced by the fit [14]  $\frac{dE}{dx} = \alpha \times E^\beta$  where, for  $dx$  in  $g/cm^2$ ,  $\alpha$  and  $\beta$  are almost pressure-independent near 1 mbar;  $\beta = 0.29$  and  $\alpha$  is fixed so to have  $dE/dx = 35$  eV/cm at 1 keV and 1 mbar. These values have been first extracted in [14] at 4 and 8.2 mbar, and later confirmed in [7] at 1 and 0.2 mbar. The angle and energy loss at each collision is determined by screened Rutherford scattering. The only involved parameter is  $r_s = 1.5r_b/2$  ( $r_b/2$  is the Bohr radius for  $He^+$ ). The values of the helium parameters  $r_s, \alpha, \beta$  are fixed by the measurement at 0.2 mbar in [7] in a way that is not affected by the reflection process discussed here, since in the 0.2 mbar case the vessel is much longer and the end wall has no effect on the examined vessel region. The cascade time has been best-fitted to  $0.4 \mu s$  in the present work.

For the simulation of Fig. 2 (bottom right) and Fig.3 we have considered 270,000 antiprotons entering the vessel with energy homogeneously distributed between 0 and 30 keV. Some preliminary simulations have been pushed to 80 keV, showing that particles between 30 and 80 keV do not introduce relevant differences in the regions of the Main and Backward Belt.

Because of the wide energy spectrum extending up to 3 MeV, the very largest part of the annihilation events occurs on the end wall after some tens of nanoseconds (time of flight). For this reason we have removed from the present data analysis the antiproton annihilations occurring in the first 250 ns. At larger times, initial-wall and end-wall annihilations affect the regions  $z < 5$  cm and  $z > 60$  cm (green areas in Fig.2, top) because of the 1 cm Gaussian uncertainty in the measurement of  $z$ , and of the huge number of these annihilations.

The scatter plot of Fig.2 (bottom right) has been simulated including propagation and multiple scattering inside the end wall, and it can be considered satisfactory. This is not only evident from the comparison of experimental and simulated scatter plots (bottom panels of Fig.2), but also from the comparison of the time distributions for events with given  $z$ . This is shown in Fig.3, where we report three subsets of the events of the scatter plots of Fig.2. These subsets correspond to (top)  $14 \text{ cm} < z < 16 \text{ cm}$ , (middle)  $40 \text{ cm} < z < 42 \text{ cm}$ , (bottom)  $56 \text{ cm} < z < 58 \text{ cm}$ . The time distributions of these subsets are reported for the experimental and for the simulated events (black and red histograms in Fig.3). Within standard statistical fluctuations, the simulation reproduces the shape and also the normalization of the experimental distributions.

The present reproduction of the data may be compared with the one of [7]. The difference introduced by including the effect of the end wall is evident, both in the scatter plot and in the  $z$ -slices.

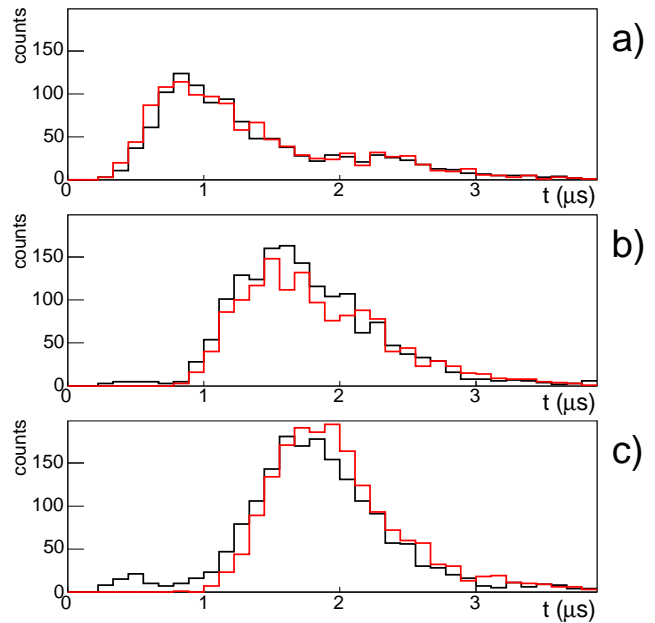


Figure 3: (Color) Comparison between experimental (black) and Monte Carlo (red) data. Time-distribution of the subsets of events corresponding to three different slices in  $z$  coordinate: (a):  $14 \text{ cm} < z < 16 \text{ cm}$ ; (b):  $40 \text{ cm} < z < 42 \text{ cm}$ ; (c):  $56 \text{ cm} < z < 58 \text{ cm}$ .

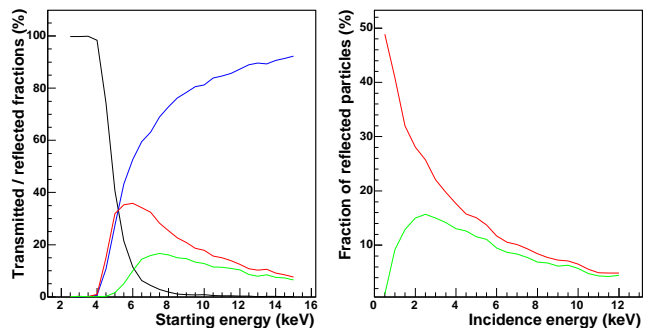


Figure 4: (Color) Simulated distributions. Left: distribution with respect to the energy at the entrance of the gas container, for antiprotons that come to rest in gas before reaching the end wall (black), that reach the end wall (blue), that are reflected by the end wall (red), that are reflected with enough energy to reach  $z < 65$  cm (green). Right: distribution with respect to the energy when hitting the aluminum wall, for antiprotons that are reflected (red), that are reflected with enough energy to reach  $z < 65$  cm (green).

#### IV. DISCUSSION

In Figs.4 and 5 the simulation code is used to study some relevant properties of the reflection process. In Fig.4 (left) we compare the dependence on the initial energy (the energy of the antiprotons when they enter the vessel) of the fraction of particles that (i) stop in helium

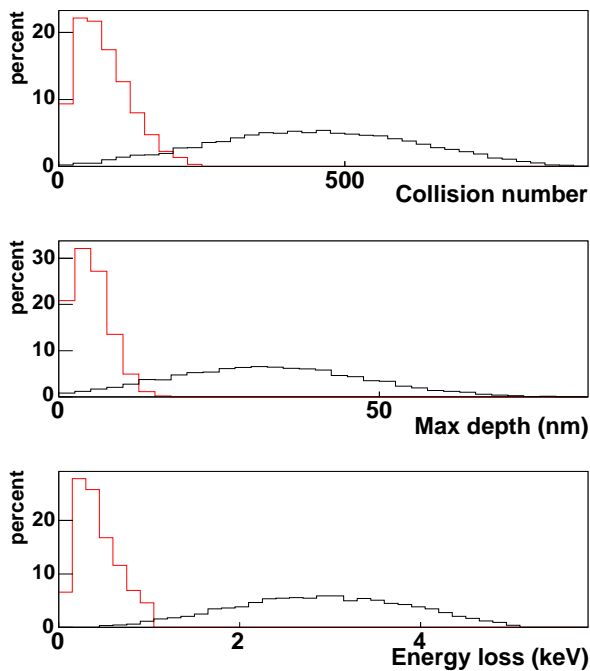


Figure 5: (Color) Relevant distributions (in percent) for in-wall features of antiprotons: in red for 1 keV energy, in black for 5 keV energy. These distributions only refer to antiprotons that are reflected. See text for details.

before reaching the end wall, (ii) come to rest in aluminum, (iii) are reflected, (iv) are reflected with enough energy (about 500 eV) to get 10 cm backward in the gas at least. In Fig.4 (right) the distributions (iii) and (iv) are considered as functions of the energy owned by the antiprotons when they hit the aluminum wall with normal incidence. Fig.5 is devoted to the behavior of the antiprotons inside aluminum. The red histograms of Fig.5 refer to 20,000 antiprotons entering aluminum with normal incidence and energy 1 keV. Of these, 7,487 are reflected. For these particles only, we show the distribution (in percentage terms) of the number of scattering events inside aluminum, of the maximum longitudinal depth reached inside the wall, and of the lost energy. The same distributions are reported in the black histograms of Fig.5 for 11,347 reflected  $\bar{p}$  out of 80,000 ones with energy 5 keV.

In Fig.5 “scattering event” means any event where the

antiproton passes within  $1.25 \text{ \AA}$  from the target nucleus. At all the energies where we have measurements of the annihilation cross section of antiprotons on some nucleus, this is many orders of magnitude smaller than the atomic-size cross section for elastic scattering. Decreasing the energy, the annihilation cross sections at low energy should follow a “1/energy” law, that is typical for inelastic processes between hadrons with opposite electric charge (see e.g. [21] and references therein). So we need to check that annihilation cross sections do not grow to a size such as to obscure elastic reflection effects. For hydrogen, deuterium and helium targets, where we have measurements at very small energies [22, 23], we have  $\sigma_{ann} \approx \frac{c^2}{v^2} \times 10^{-27} \text{ cm}^2$ , where  $v$  is the antiproton velocity and  $c$  is the speed of light. Assuming that in the aluminum case the annihilation cross section is  $N$  times larger than in the helium or hydrogen cases, and taking  $\sigma_{el} = (1.25 \text{ \AA})^2$ , we have  $\sigma_{ann}/\sigma_{el} \approx 2 \cdot 10^{-6} N/E$ , for  $E$  expressed in keV. No data or theory gives us elements to imagine that  $N$  may overcome 100 in magnitude. This means that both at 1 keV and 5 keV the number of scattering events reported in Fig.5 corresponds to a path that is much shorter than the average annihilation path.

The physics emerging from these data is simple: at the distance scale of the nuclear radius it is fair to consider antiprotons as “destructive” particles, but for an antiproton with energy 1-10 keV the probability of finding itself within such a distance from the nucleus is several orders of magnitude smaller than the probability of being deflected by an angle 20 degrees. After 10 such collisions the memory of the initial direction would be completely lost, and 50% of the antiprotons would be backward directed. At energy 5 keV we do not have so many large angle collisions, but their number is anyway large enough to allow a relevant fraction of the antiprotons to be reflected. The Monte Carlo simulation shows that *multiple* scattering (with angles  $10^\circ - 40^\circ$ ) dominates the reflection process at the energies that are central here (some keV). At energies  $< 1 \text{ keV}$  single scattering with angle  $> 90^\circ$  becomes relevant too.

In the near future, the systematic experimental study of antimatter reflection can be realized at AD at CERN, for example by the ASACUSA Collaboration [24], or at the future low energy antiproton facility FLAIR at GSI [25].

[1] T. Walcher, Ann. Rev. Nucl. Part. Sci. **38**, 67 (1988).  
 [2] M. Amoretti *et al.*, Nature **419**, 456 (2002).  
 [3] G. Gabrielse *et al.*, Phys. Rev. Lett. **89**, 213401 (2002).  
 [4] T. Yamazaki *et al.*, Nature **361**, 238 (1993).  
 [5] N. Zurlo *et al.*, Phys. Rev. Lett. **97**, 153401 (2006).  
 [6] E. Lodi Rizzini, L. Venturelli & N. Zurlo, ChemPhysChem **8**, 1145 (2007).  
 [7] A. Bianconi *et al.*, Phys. Rev. A **70**, 032501 (2004).

[8] E. Rutherford, Philos. Mag. **21**, 669 (1911).  
 [9] A.P. Mills Jr., Phys. Rev. Lett. **41**, 1828 (1978).  
 [10] D.B. Cassidy & A. P. Mills Jr., Nature **449**, 195 (2007).  
 [11] A. Adamo. *et al.*, Sov. J. Nucl. Phys. **55**, 1732 (1992).  
 [12] A. Zenoni. *et al.*, Nucl. Instr. and Meth. A **447**, 512 (2000).  
 [13] A. Bertin *et al.*, Phys. Rev. A **54** 5441 (1993).  
 [14] M. Agnello *et al.*, Phys. Rev. Lett. **74** 371 (1995).

- [15] E. Lodi Rizzini *et al.*, Phys. Rev. Lett. **89**, 183201 (2002).
- [16] E. Lodi Rizzini *et al.*, Phys. Lett. B **599**, 190 (2004).
- [17] S.P. Møller *et al.*, Phys. Rev. Lett. **93**, 042502 (2004).
- [18] P. Sigmund & A. Schinner, Eur. Phys. J. D **12**, 425 (2000).
- [19] D.L. Morgan Jr, Hyperf. Int. **44** 399 (1988).
- [20] J.S. Cohen, Phys. Rev. A **56**, 3583 (1997).
- [21] A. Bianconi *et al.*, Phys. Lett. B **483**, 353 (2000).
- [22] A. Zenoni *et al.*, Phys. Lett. B **461**, 405 (1999).
- [23] A. Bertin *et al.*, Phys. Lett. B **369**, 77-85 (1996).
- [24] R.S. Hayano *et al.*, SPSC-SR-027 ; CERN-SPSC-2008-002 (2008).
- [25] <http://www.oeaw.ac.at/smi/flair/>